Frontiers in Bioscience Landmark

Front. Biosci. (Landmark Ed) **2026**; 31(11): 51637
https://doi.org/10.31083/FBL51637

Original Research

Kaempferol Suppresses the EGFR/VEGFR2 Axis to Augment Therapeutic Efficacy in Gastric Cancer Through Coordinated Inhibition of the PI3K/AKT/mTOR Pathway

Hailong Li[1,2,3,†], Meng Wang[2,†], Lihua Shao[2], Rong Su[2], Yonghua Hu[2], Hongwei Wang[4,*]

[1]Department of Geriatrics, Shenzhen Hospital of Integrated Traditional Chinese and Western Medicine, 518104 Shenzhen, Guangdong, China
[2]Department of Internal Medicine, First School of Clinical Medicine, Gansu University of Chinese Medicine, 730000 Lanzhou, Gansu, China
[3]Department of Research Management, Affiliated Hospital of Gansu University of Chinese Medicine, 730000 Lanzhou, Gansu, China
[4]Department of Laboratory Medicine, Affiliated Hospital of Gansu University of Chinese Medicine, 730000 Lanzhou, Gansu, China
*Correspondence: whw197710@163.com (Hongwei Wang)
[†]These authors contributed equally.
Academic Editors: Kota V. Ramana and Amedeo Amedei
Submitted: 9 March 2026 Revised: 30 June 2026 Accepted: 31 July 2026 Published: 11 November 2026

Abstract

Objective: We combined network pharmacology, molecular docking, and *in vitro* assays to clarify the anti-gastric cancer (GC) mechanisms of kaempferol. **Methods:** Potential targets of kaempferol and GC-related genes were identified via public database screening. Protein-protein interaction (PPI) networks, Kyoto Encyclopedia of Genes and Genomes (KEGG) pathway, and Gene Ontology (GO) enrichment analyses were constructed. Molecular docking and 100-ns molecular dynamics (MD) simulations validated binding stability. *In vitro* assays included 3-(4,5-Dimethylthiazol-2-yl)-2,5-diphenyltetrazolium bromide (MTT) for viability, zero-interaction potency (ZIP) model synergy evaluation with erlotinib/apatinib, flow cytometry for apoptosis/cell cycle, Reverse Transcription Quantitative Polymerase Chain Reaction (RT-qPCR), and Western blotting. **Results:** Network analysis revealed 1879 potential GC-related targets, of which 48 intersected with kaempferol's predicted targets. Kaempferol (40–200 μM) significantly inhibited GC cell proliferation ($p < 0.01$) and exhibited synergistic effects when combined with erlotinib (ZIP score: 1.269–3.687) or apatinib (ZIP score: 2.576–3.894). Kaempferol also induced dose-dependent apoptosis and G0/G1 phase arrest ($p < 0.01$). Mechanistically, kaempferol suppressed phosphorylation of Epidermal Growth Factor Receptor (EGFR), Phosphoinositide 3-Kinase (PI3K), Ak Strain Transforming (AKT), and Mechanistic Target of Rapamycin (mTOR), upregulated proapoptotic proteins (Bcl-2–Associated X Protein (Bax), p53, p21), and downregulated antiapoptotic B-Cell Lymphoma 2 (Bcl-2) and cell cycle regulators (Cyclin-Dependent Kinase 4 (CDK4), CDK6) ($p < 0.01$). **Conclusion:** Kaempferol exerts antitumor effects primarily via suppressing the EGFR/PI3K/AKT/mTOR pathway, leading to cell cycle arrest and apoptosis, and enhances the efficacy of EGFR/Vascular Endothelial Growth Factor Receptor (VEGFR)-targeted therapies, supporting its potential as a plant-derived chemosensitizer for GC.

Keywords: network pharmacology; kaempferol; gastric cancer; molecular docking; PI3K/AKT/mTOR signaling pathway

1. Introduction

Gastric cancer (GC) represents the fifth most prevalent malignancy globally [1] and ranks fifth in morbidity and fourth in mortality [2], five-year survival rates in most countries range from 20% to 40% [1]. Previous studies/reviews have summarized that herbal medicines and their extracts can mitigate adverse effects in patients undergoing radiotherapy and chemotherapy [3] and sensitize tumors to enhance the efficacy of conventional treatments, including chemotherapy, targeted therapy, and immunotherapy [4]. Preclinical studies indicate that kaempferol can modulate chemotherapy-responsive pathways—such as TS/Akt, NLRP3-mediated pyroptosis, and 5-FU/oxaliplatin sensitivity in gastrointestinal models—supporting its potential as a chemosensitizer, although direct gastric-cancer combination studies remain limited [5,6].

Preclinically, kaempferol shows chemosensitizing potential through pleiotropic targeting of oncogenic cascades [7,8]. Recent studies have suggested that kaempferol may enhance the susceptibility of pancreatic tumor cells to erlotinib through suppression of the EGFR/PI3K/AKT signaling pathway [9]. Despite known antitumor activities in GC, the precise mechanisms behind kaempferol's effects are incompletely understood, and its combined action with EGFR inhibitor erlotinib or Vascular Endothelial Growth Factor Receptor (VEGFR) inhibitor apatinib has not been investigated. Therefore, by combining network pharmacology, molecular docking, molecular dynamics simulation, and synergistic activity testing, this study seeks to clarify the function of kaempferol as a chemosensitizer in GC treatment.

Copyright: © 2026 The Author(s). Published by IMR Press.
This is an open access article under the CC BY 4.0 license.

Publisher's Note: IMR Press stays neutral with regard to jurisdictional claims in published maps and institutional affiliations.

2. Materials and Methods

2.1 Identification of the Targets of Kaempferol on GC

The Structure Data File (SDF)-format chemical structure of kaempferol was converted into a mol2 format utilizing Open Babel software (https://openbabel.org/, Manufactured by Open Babel open-source project) and submitted to SwissTargetPrediction [10] for prediction. Gene symbols were standardized using the UniProt database [11] following the consolidation of all compound targets. Disease targets associated with GC were retrieved by querying the human gene annotation resource GeneCards with the search term "gastric cancer".

2.2 Venn Diagram and Protein Interaction Network Diagram

Kaempferol and GC intersection targets were loaded into the Search Tool for the Retrieval of Interacting Genes/Proteins (STRING) database (https://string-db.org/). The steps involved importing the intersection targets of kaempferol and GC targets into the STRING database, setting the species to "Homo sapiens", and setting the minimal interaction score to "0.400" in order to hide the free points and create a protein interaction network. In order to do topological analysis and visualization, Cytoscape software 3.9.0 (Seattle, WA, USA) was used to import all network data [12].

2.3 GO and KEGG Enrichment Analysis

The cluster analysis tool on the Metascape platform was used to conduct GO and Kyoto Encyclopedia of Genes and Genomes (KEGG) pathway studies [13]. The KEGG pathway enrichment study employed a *p*-value threshold of less than 0.01 as the standard for statistical significance. The Weishengxin web platform was used to visualize the analysis results.

2.4 Analysis of Molecular Docking and Dynamics Simulations

Molecular docking and molecular dynamics simulations were used to examine the binding activity of kaempferol to important targets. While protein structures were retrieved from the Protein Data Bank (PDB), the kaempferol SDF file was acquired via PubChem. After evaluating the binding postures by molecular docking with AutoDock Vina, the results were visualized. GROMACS 2022 was then used to do molecular dynamics (MD) simulations. Kaempferol was subjected to the General AMBER Force Field (GAFF), whereas the protein was subjected to the AMBER14SB force field and the TIP3P water model. Periodic boundary conditions under constant temperature (298 K) and pressure (1 bar) were applied to the system; the V-rescale and Berendsen methods were used to maintain temperature and pressure, respectively. The LINear Constraint Solver (LINCS) technique with a 2 fs integration step was used to restrict hydrogen bonds, and the particle mesh Ewald method with a 1.2 nm cutoff was used to determine electrostatic interactions. A 100 ns production MD simulation was carried out after 100 ps of Constant Number of particles, Volume, and Temperature ensemble (NVT) and Constant Number of particles, Pressure, and Temperature ensemble (NPT) equilibration, with conformations saved every 10 ps. Lastly, PyMOL (https://www.pymol.org/) and VMD (https://www.ks.uiuc.edu/Research/vmd/) were used to analyze the trajectory, and the g-mmpbsa program was used to calculate the binding free energy.

2.5 Cell Lines and Materials

The human gastric cancer cell lines HGC-27 (Cat. No. [TCH-C202]; Hysigen Biosciences, Suzhou, Jiangsu, China) and MKN-45 (Cat. No. 06.0209; EallBio Biotechnology Co., Ltd., Beijing, China) were used in this study. Both cell lines were authenticated by STR (short tandem repeat) profiling and tested negative for mycoplasma. HGC-27 cells were cultured in RPMI-1640 medium supplemented with 10% fetal bovine serum (FBS) and 100 U/mL penicillin and 100 µg/mL streptomycin. MKN-45 cells were cultured in RPMI-1640 medium supplemented with 10% FBS and 1% penicillin-streptomycin (100 U/mL penicillin and 100 µg/mL streptomycin). All cells were maintained at 37 °C in a humidified incubator with 5% CO_2. Cells within passages 3–5 after resuscitation were used for experiments. The kits and reagents listed below were acquired from different vendors: fetal bovine serum (batch number: 22070701, Zhejiang Tianhang Biotechnology Co., Ltd., China); RPMI-1640 culture medium (batch number: AH29755233, HyClone company, USA); Qinghai Streptomycin double antibody (batch number: CR2102024, Wuhan Sewell Biotechnology Co., Ltd., China); Erlotinib (HY-50896, MedChemExpress, Monmouth Junction, NJ, USA); Apatinib (H20140103, Jiangsu Hengrui Pharmaceuticals Co., Ltd., Lianyungang, Jiangsu, China); EGF (Cat. No. 92701ES76, Yeasen, Shanghai, China); apoptosis detection kit and cell cycle kit (batch numbers: A11015 and A10952, Hangzhou MULTI-SCIENCES Biotechnology Co., Ltd., China respectively); ultrasensitive enhanced chemiluminescence (ECL) chemiluminescence kit (batch number: 20220511, Suzhou Xinsemi Biotechnology Co., Ltd., China); total RNA extraction kit (batch number: M321952, Shanghai Yeasen Biotechnology Co., Ltd., China); and Horseradish Peroxidase (HRP)-labeled goat anti-rabbit (batch number: 226730627, Beijing Zhongshan Jinqiao Biotechnology Co., Ltd., China). Several reagents, including radioimmunoprecipitation assay (RIPA) (Cat. No. R0010, Lot No. 20220310; Beijing Solarbio Science & Technology Co., Ltd., Beijing, China) lysate (batch number: 20220310, Beijing Solarbio company, China), phenylmethylsulfonyl fluoride (batch number: 20220107, Beijing Solarbio company, China), bicinchoninic acid (BCA) protein quantitative detection kit (batch number: 20220830, Beijing Solarbio com-

pany, China), protein phosphatase inhibitor (batch number: 20220605, Beijing Solarbio company, China), MTT (batch number: 1123A051, Beijing Solarbio company, China), and Kaempferol (batch number: SK8030, HPLC, 99%, Beijing Solarbio company, China). Antibodies against GAPDH (batch number: #62u9022, Affinity company, USA), p21 (Cat. No. YT3497, ImmunoWay Company, San Jose, CA, USA), AKT (batch number: #34d5362, Affinity company, USA), PI3K (batch number: #54f8512, Affinity company, USA), EGFR (batch number: #45u9052, Affinity company, USA), p-PI3K (batch number: #51u8853, Affinity company, USA), and p-mTOR (batch number: #55y1643, Affinity company, USA); CDK4 (batch number: B7701, Immunoway company, USA), CDK6 (batch number: B1301, Immunoway company, USA), p-AKT (batch number: B9001, Immunoway company, USA), Bcl-2 (batch number: B7001, Immunoway company, USA), VEGFR2 (Catalog: YM8529, Immunoway company, USA), VEGFA (Catalog: YM8345, Immunoway company, USA), BAX (batch number: B9101, Immunoway company, USA), and mTOR (batch number: B8501, Immunoway company, USA); and p-EGFR (batch number: GR3333718-8, Abcam company, USA). PCR primers were synthesized by Beijing Biomed Gene Technology Co., Ltd. Kaempferol was sterilized by filtration through a 0.22 μm filter membrane before use.

2.6 Detection of Cell Viability

For the purpose of evaluating cytotoxicity, the logarithmic growth phase GC cell lines MKN-45 and HGC-27 were seeded in 96-well plates (1×10^4 cells/well) and exposed to kaempferol solution at final concentrations of 20, 40, 60, 80, 100, 120, 160, and 200 μM. To find the IC_{50}, cells were also exposed to erlotinib or apatinib at final concentrations of 1, 5, 10, 20, 40, 60, 80, and 100 μM. 20 μL of MTT solution (5 mg/mL) was applied and incubated for 4 hours following 24, 48, and 72 hours of incubation. Formazan crystals were then dissolved by thoroughly shaking each well after adding 150 μL of Dimethyl Sulfoxide (DMSO). A microplate reader was used to detect the optical density (OD) at 570 nm, and the cell growth rate was computed as follows: Proliferation rate (%) is equal to [(OD_drug-treated – OD_blank) / (OD_control – OD_blank)] × 100%. The tested concentration range was 0–100 μM. IC_{50} values exceeding the highest tested concentration (100 μM) were obtained by extrapolation of the nonlinear regression curve beyond the experimentally evaluated range and are denoted as extrapolated.

2.7 Synergistic Effects of Kaempferol Combined With Erlotinib and Apatinib

GC cells in the logarithmic growth phase were treated with different concentrations of erlotinib (10.625, 21.25, 42.5, 85, 127.5 μM), kaempferol (5, 10, 20, 40, 60 μM), and apatinib (4.75, 9.5, 19, 38, 57 μM), either alone or in combination, and cell viability was assessed. The zero-interaction potency (ZIP) model was utilized to construct drug synergy scores using the SynergyFinder web tool (https://synergyfinder.fimm.fi), with the inhibition index computed as (100-% cell viability). A ZIP synergy score higher than zero was considered indicative of synergism [14]. The concentration ranges for kaempferol (5–60 μM), erlotinib (10.625–127.5 μM), and apatinib (4.75–57 μM) were selected on the basis of their IC_{50} values in MKN-45 and HGC-27 cells. Kaempferol was specifically applied at 20, 40, and 80 μM in subsequent apoptosis and cell cycle assays, which span sub-IC_{50} to near-IC_{50} levels relative to the 48-h IC_{50} values (HGC-27: 39.84 μM; MKN-45: 103.9 μM). This design ensures detectable combinatorial effects and conforms to the requirements of ZIP synergy analysis. Although baseline sensitivities differ (e.g., HGC-27 IC_{50}: 22.64–71.40 μM vs. MKN-45: 77.21–134.7 μM), standardized ranges enable direct comparisons of synergy scores across cell lines.

2.8 Detection of Apoptosis and Cell Cycle Assay

MKN-45 and HGC-27 cells were exposed to kaempferol (20, 40, and 80 μM) for 48 hours during the logarithmic growth phase. Cells were then collected and prepared for cell cycle and apoptosis examination by BD FACSVerse™ Cell Analyzer (BD Biosciences, San Jose, CA, USA). For both apoptosis and cell cycle analyses, a standardized gating strategy was applied to ensure data accuracy and reproducibility: (1) a forward/side scatter (FSC/SSC) gate was used to select the target cell population and exclude cellular debris; (2) a singlet gate was applied by plotting FSC-H versus FSC-A (or SSC-H versus SSC-A) to exclude doublets and cell aggregates. For apoptosis detection, cells were washed with Phosphate Buffered Saline (PBS), resuspended in Annexin V binding buffer, and stained with Annexin V-fluorescein isothiocyanate (FITC) and propidium iodide (PI) for 15 minutes in the dark. Prior to data acquisition, fluorescence compensation settings for Annexin V-FITC and PI were calibrated using unstained and single-color control samples (unstained, Annexin V-FITC only, and PI only) to correct for spectral overlap. Quadrant threshold settings were established based on the unstained control to accurately distinguish viable, early apoptotic, late apoptotic, and necrotic cells. For cell cycle analysis, parallel samples were frozen, permeabilized, and stained with a propidium iodide solution for 30 minutes in the dark. Cell cycle distribution was determined using flow cytometry, and data were analyzed using ModFit LT Software v4.1.7 (Verity Software House, Topsham, ME, USA).

2.9 RNA Extraction and Quantitative Real-Time PCR (qPCR)

Kaempferol (20, 40, and 80 μM) was applied to MKN-45 and HGC-27 cells for 24 hours. In accordance with the

Table 1. Primer sequences for real time fluorescence quantitative PCR.

Gene	Forward sequence (5′- 3′)	Reverse sequence (5′- 3′)	Product size (bp)
Bcl-2	ATGTGTGTGGAGAGCGTCAAC	ACAGCCAGGAGAAATCAAACAG	178 bp
Bax	ACTGAAGCGACTGATGTCC	TTCCAGATGGTGAGTGAGG	121 bp
CDK4	CCTTCCCATCAGCACAGTTC	TCAAACACCAGGGTTACCTTG	138 bp
CDK6	CGTGGTCAGGTTGTTTGATG	CCTTTATGGTTTCAGTGGGC	113 bp
TP53	CAGCACATGACGGAGGTTGT	TCATCCAAATACTCCACACGC	125 bp
p21 (*CDKN1A*)	TGTGGACCTGTCACTGTCTTG	TCCTCTTGGAGAAGATCAGCCG	264 bp
GAPDH	CATCACCATCTTCCAGGAG	CTTGAGGCTGTTGTCATACTTC	217 bp

PCR, polymerase chain reaction; *Bcl-2*, B-cell lymphoma 2; *Bax*, *Bcl-2*-associated X protein; CDK4, cyclin-dependent kinase 4; GAPDH, glyceraldehyde-3-phosphate dehydrogenase.

manufacturer's instructions, total RNA was extracted using an RNA extraction kit. A reverse transcription kit was used to create complementary DNA (cDNA) from 1 µg of total RNA. A Bio-RAD CFX-96 real-time PCR machine was used for qPCR amplification. To confirm the amplification's specificity, a dissociation curve analysis was performed. The $2^{-\Delta\Delta Ct}$ technique was used to calculate relative mRNA expression levels, and GAPDH was used as the endogenous reference gene for standardization. All experiments were performed with three independent biological replicates. The primer sequences are listed in Table 1.

2.10 Western Blot Analysis

Following treatment of GC cells with kaempferol (20, 40, and 80 µM) for 48 hours, RIPA lysis buffer supplemented with 1 mM phenylmethylsulfonyl fluoride (PMSF) and 1× phosphatase inhibitor cocktail was used to extract total proteins. A BCA assay was used to calculate the protein content. SDS-polyacrylamide gel electrophoresis (SDS-PAGE) was used to separate equal amounts of protein (20 µg per lane) on gels of suitable concentrations (6%, 10%, or 12%) according to the molecular weights of the target proteins. The gels were then electrophoretically transferred onto Polyvinylidene difluoride (PVDF) membranes. For 1.5 hours at room temperature, membranes were blocked using 5% (w/v) skim milk in Tris-buffered saline containing 0.1% Tween-20 (TBST). Membranes were then treated with particular primary antibodies (such as anti-AKT (#34d5362, Affinity, USA), anti-p53 (YM8533, Immunoway, USA), anti-VEGFR2 (YM8529, Immunoway, USA), anti-VEGFA (YM8345, Immunoway, USA) and anti-EGFR (#45u9052, Affinity, USA)) diluted in TBST containing 5% Bovine Serum Albumin (BSA) for an entire night at 4 °C. After three TBST washes, membranes were incubated for two hours at room temperature with an HRP-conjugated secondary antibody (such as goat anti-rabbit IgG, B0101, Immunoway, USA) diluted in blocking solution. An ECL detection system was used to view protein bands. ImageJ software (version 1.54u8, National Institutes of Health, Bethesda, MD, USA) was used to quantify band intensities, which were then normalized to GAPDH as a loading control.

2.11 Statistical Methods

GraphPad Prism 8.0 was used to analyze the data, and the means ± standard deviations ($\bar{x} \pm s$) are used to express the experimental results. The experimental data was compared between groups using one-way analysis of variance (ANOVA) and the Least Significant Difference (LSD), Tukey, or Dunnett technique; $p < 0.05$ was deemed statistically significant.

3. Results

3.1 Collection of Kaempferol Targets and Disease Targets

The Swiss Target Prediction service was used to forecast potential kaempferol targets. Using the term "gastric cancer", 1879 possible disease targets were found in the GeneCards database. For kaempferol, 100 possible targets were found; of these, 48 overlapped with GC targets, indicating the intersection targets for more investigation (Fig. 1A).

3.2 Protein-Protein Interaction (PPI) Network Construction

Cytoscape 3.9.0 was used to analyze and visualize the TSV files that were produced after the previously described 48 intersection targets were put into the STRING database to create a PPI network. There were 261 edges and 48 nodes in the final PPI network. Each node's degree value was determined; higher values denoted increased connection and possible functional significance. AKT1, Interleukin-6 (IL-6), Vascular Endothelial Growth Factor A (VEGFA), SRC Proto-Oncogene (SRC), EGFR, Heat Shock Protein 90 Alpha Family Class A Member 1 (HSP90AA1), Signal Transducer and Activator of Transcription 3 (STAT3), Mitogen-Activated Protein Kinase 3 (MAPK3), Jun Proto-Oncogene (JUN), and mTOR were determined to be the top ten core targets based on degree values. To show the relationships, a compound-target network was built (Fig. 1B).

3.3 GO and KEGG Pathway Enrichment Analysis

The Metascape platform was used to perform KEGG and GO enrichment studies on the overlapping targets between kaempferol and GC. 116 substantially enriched cancer-related pathways were found using KEGG pathway

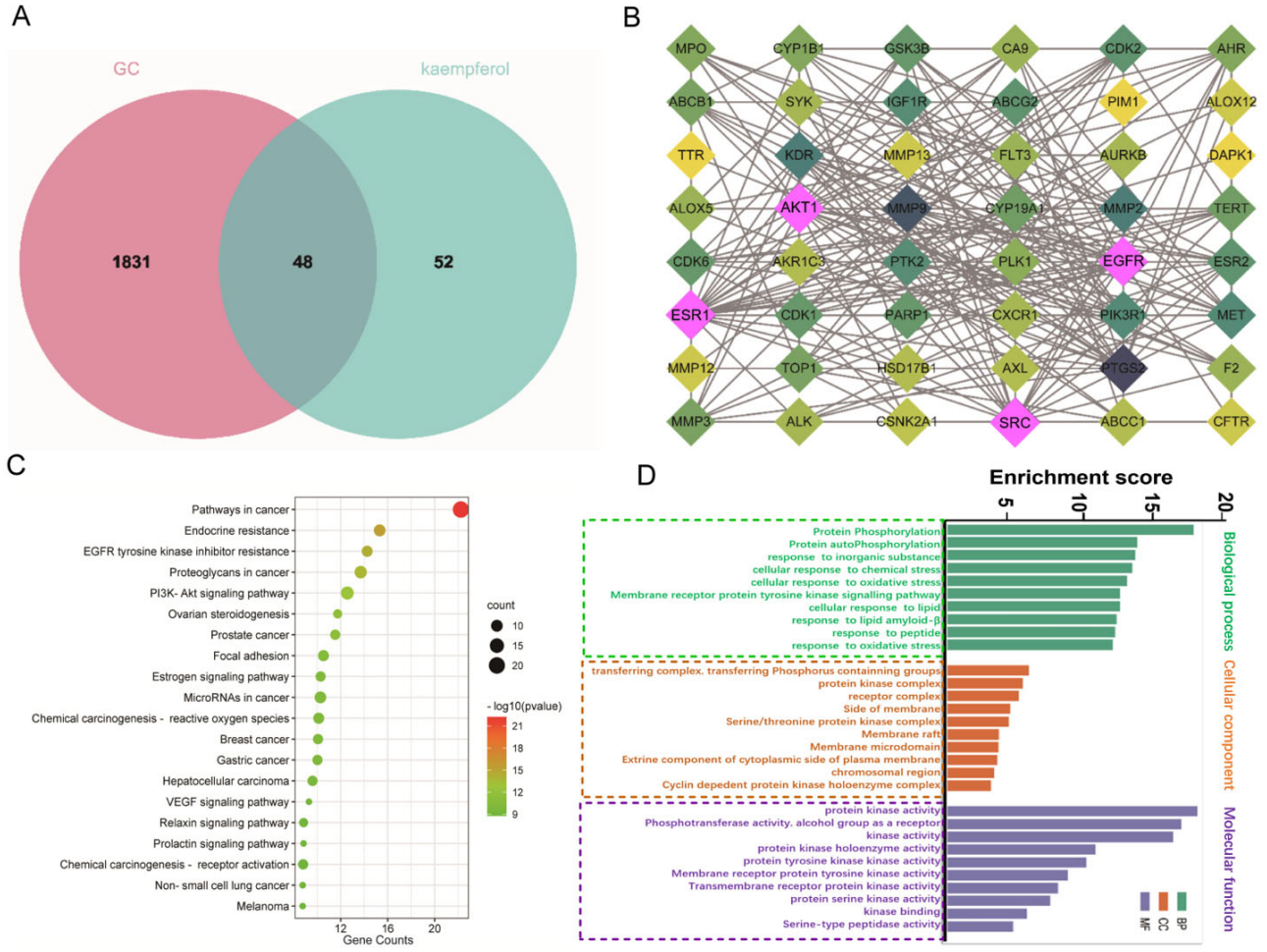


Fig. 1. Network pharmacology of kaempferol intervention on gastric cancer (GC), Gene Ontology (GO) and Kyoto Encyclopedia of Genes and Genomes (KEGG) enrichment analysis. (A) Venn diagram showing overlap between 100 kaempferol-predicted targets and 1879 GC-related targets, with 48 intersecting targets retained for subsequent analysis. (B) Compound-target interaction network of kaempferol and GC intersecting targets, containing 48 nodes and 261 edges; node size corresponds to degree value, larger nodes indicate higher connectivity. (C) Bubble plot of the top 20 enriched KEGG pathways, with bubble size representing gene count and color representing significance level (−log10 *p*-value). (D) Bar chart of top 10 enriched Gene Ontology (GO) terms across biological process (BP), cellular component (CC), and molecular function (MF) categories.

analysis. Key pathways included EGFR tyrosine kinase inhibitor resistance, the PI3K-Akt signaling system, and the VEGF signaling pathway. The top 20 pathways, ranked by *p*-value, were shown in a bubble chart. GO analysis identified 77 molecular functions (MF), 455 biological processes (BP), and 41 cellular components (CC). For bar chart representation, the top ten terms in each category that were significantly enhanced were chosen. Protein kinase activity and transmembrane receptor protein tyrosine kinase activity were the main factors associated with enriched MF keywords. The cellular reaction to oxidative stress and protein phosphorylation were both heavily influenced by BP parameters. Membrane rafts, membrane microdomains, and receptor complexes were primarily linked to CC keywords (Fig. 1C,D).

3.4 Molecular Docking and Dynamics Simulations Reveal Stable Binding of Kaempferol to Key Targets

The binding mechanism and stability of kaempferol with important targets (AKT1, EGFR, mTOR, and PI3K) were assessed using molecular docking and dynamics simulations. During the first 20 ns of the simulation, the protein-ligand complexes' root mean square deviation (RMSD) showed notable variations (Fig. 2Aa,Ba,Ca,Da), suggesting conformational changes of the small molecule inside the binding pocket. The RMSD plateaued after this equilibration time, indicating that kaempferol was securely bound at the target location and the system had reached a stable state (Fig. 2Aa,Ba,Ca,Da). Consistent with these observations, the root mean square fluctuation (RMSF) and radius of gyration (Rg) analyses indicated the local flexibility and overall compactness of the complexes during the simula-

Table 2. The binding free energy components (kcal·mol^{-1}) of kaempferol with target proteins calculated by MM-PBSA.

Complex	$\triangle E_{vdw}$	$\triangle E_{ele}$	$\triangle E_{pol}$	$\triangle E_{nonpol}$	$\triangle E_{MMPBSA}$	$-T\triangle S$	$\triangle G_{bind}$
akt17myx-Kaempferol	–95.026 ± 4.492	–15.188 ± 1.045	70.462 ± 3.278	–12.616 ± 0.347	–52.368 ± 2.1	27.88 ± 4.935	–24.488 ± 6.878
EGFR-Kaempferol	–155.435 ± 1.754	–30.15 ± 2.331	129.608 ± 3.557	–17.74 ± 0.028	–73.717 ± 3.124	14.502 ± 1.623	–59.215 ± 4.397
mTOR7ped-Kaempferol	–106.66 ± 2.708	–29.756 ± 1.485	110.454 ± 1.906	–12.944 ± 0.376	–38.906 ± 3.09	13.994 ± 0.744	–24.913 ± 2.414
PI3K3i5s-Kaempferol	–159.842 ± 2.733	–118.885 ± 7.828	160.752 ± 8.115	–21.469 ± 0.089	–139.444 ± 2.563	19.923 ± 2.248	–119.52 ± 1.668

Notes: $\triangle G_{bind} = \triangle E_{vdw} + \triangle E_{ele} + \triangle E_{pol} + \triangle E_{nonpol} - T\triangle S$ (kcal·mol^{-1}). RMSD, Root mean square deviation; Rg, Radius of gyration; SASA, Solvent accessible surface area. ΔE_{vdw}, van der Waals interaction energy; ΔE_{ele}, electrostatic interaction energy in vacuum; ΔEpolar, polar solvation energy; ΔEnonpolar, non-polar solvation energy (representing hydrophobic interaction). ΔEMMPBSA is the sum of ΔE_{ele}, ΔE_{vdw}, ΔEpolar, and ΔEnonpolar. ΔGbind (Gibbs binding energy) is the sum of ΔEMMPBSA and –TΔS. Due to the large calculation error of –TΔS, this term is often excluded when comparing binding energies, and ΔEMMPBSA is directly used as the binding energy. Additionally, because of the significant error in calculating ΔEpolar, the main focus is on the other energy components (ΔE_{ele}, ΔE_{vdw}, and ΔEnonpolar).

tion (Fig. 2Ac,Bc,Cc,Dc,Ab,Bb,Cb,Db). The convergence of the distance between kaempferol and the protein backbone (or binding site center) after 20 ns provided additional evidence for this stability (Fig. 2Ad,Bd,Cd,Dd). The stable binding mode and specific interacting residues between kaempferol and the target proteins were further visualized and confirmed by molecular docking interactions and trajectory superposition (Fig. 2Aj,Bj,Cj,Dj,Af,Bf,Cf,Df). A sustained contact between kaempferol and the proteins was confirmed by energetic analyses that focused on van der Waals (VDW) and electrostatic (ELE) interactions, which are important components of binding energy excluding solvation. These analyses revealed stable profiles throughout the simulation trajectory (Fig. 2Ag,Bg,Cg,Dg). The Molecular Mechanics Poisson Boltzmann Surface Area (MM-PBSA) method was used to calculate binding free energy based on the stable trajectory (Table 2). High binding affinity was shown by docking scores that were less than –5.0 kcal·mol^{-1} for all important targets. As illustrated in the molecular docking interaction diagrams (Fig. 2Aj,Bj,Cj,Dj), kaempferol formed stable hydrogen bonds and hydrophobic interactions with key residues in the active sites of AKT1, EGFR, mTOR, and PI3K.

As shown in Table 2, the van der Waals interaction energy (ΔE_{vdw}) contributed more favorably to binding than the electrostatic interaction (ΔE_{ele}), and both were more favorable than the hydrophobic interaction (ΔEnonpol). These results indicate that van der Waals forces are the dominant contributor to the binding energy, electrostatic interactions play a secondary role, and hydrophobic interactions provide a supplementary contribution.

3.5 Kaempferol Inhibits the Proliferation of Gastric Cancer Cells

Kaempferol at final concentrations of 40, 60, 80, 100, 120, 160, and 200 μM reduced cell proliferation in a dose- and time-dependent way ($p < 0.05$) after 24, 48, and 72 hours of treatment, according to MTT data. In MKN-45 cells, kaempferol had IC_{50} values of 134.7 μM (24 hours), 103.9 μM (48 hours), and 77.21 μM (72 hours). The IC_{50} values of kaempferol intervention in HGC-27 cells following treatment at 20–100 μM were 71.40 μM (24 h), 39.84 μM (48 h), and 22.64 μM (72 h) in a time-dependent manner ($p < 0.05$). When compared to the control, all concentrations above 20 μM significantly inhibited cell growth ($p < 0.05$), suggesting that the rate of proliferation decreased as the kaempferol concentration rose (Fig. 3A,B).

The IC_{50} values of erlotinib in GC MKN-45 cells were 142.8 μM (24 h), 101.2 μM (48 h), and 69.85 μM (72 h). The IC_{50} values of erlotinib in HGC-27 GC cells were 138.3 μM (24 h), 84.77 μM (48 h), and 38.14 μM (72 h). The IC_{50} values of apatinib in GC MKN-45 cells were 133.3 μM (24 h), 118.0 μM (48 h), and 70.73 μM (72 h). The IC_{50} values of apatinib in HGC-27 GC cells were 138.9 μM (24 h), 38.14 μM (48 h), and 17.32 μM (72 h). The concentrations of apatinib and erlotinib were based on our previously determined IC_{50} values for the synergistic effects of Marsdenia tenacissima combined with erlotinib and apatinib [15].

3.6 Synergistic Effects of Kaempferol With Erlotinib and Apatinib on GC Cell Proliferation

In order to evaluate the synergistic effects, a range of concentrations of apatinib (4.75, 9.5, 19, 38, and 57 μM), erlotinib (10.625, 21.25, 42.5, 85, and 127.5 μM), and kaempferol (5, 10, 20, 40, and 60 μM) were applied to both GC cell lines (Fig. 3C–F). These ranges encompass subinhibitory concentrations (approximately 20–50% of the IC_{50}) to ensure detectable combinatorial effects, consistent with the requirements of ZIP synergy analysis. The combination of kaempferol and erlotinib exhibited synergistic effects in both cell lines, with ZIP synergy scores of 1.269 in HGC-27 cells and 3.687 in MKN-45 cells (Fig. 3C,D). Similarly, the combination of kaempferol and apatinib was synergistic, yielding ZIP scores of 3.894 in HGC-27 cells and

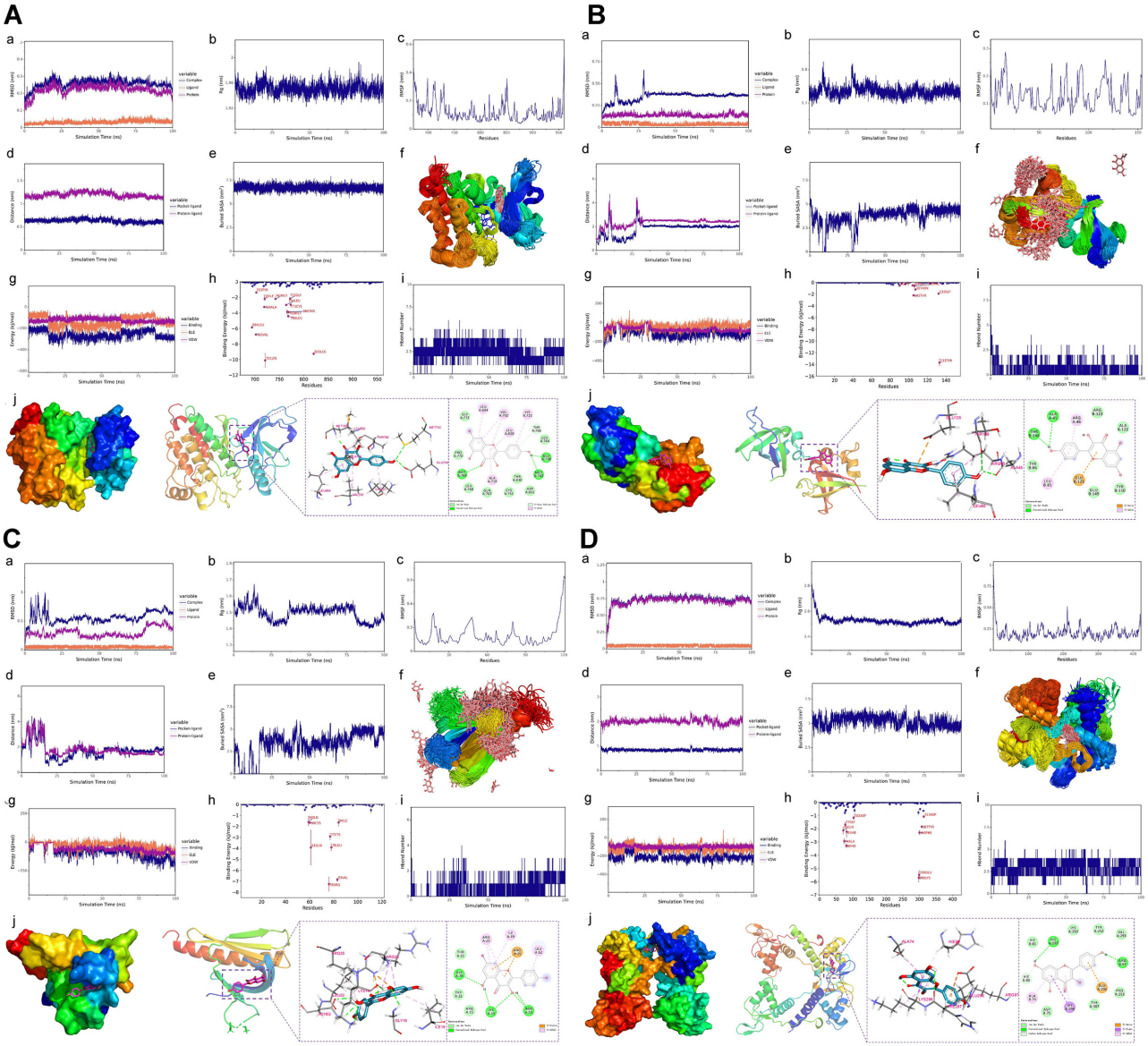


Fig. 2. Molecular docking and 100-ns molecular dynamics (MD) simulation results of kaempferol binding to four core targets. (A) AKT serine/threonine kinase 1 (AKT1), (B) epidermal growth factor receptor (EGFR), (C) mechanistic target of rapamycin (mTOR), (D) phosphoinositide 3-kinase (PI3K). Subpanels include: (a) root-mean-square deviation (RMSD) of complex/protein/ligand; (b) radius of gyration (Rg) of the complex; (c) root-mean-square fluctuation (RMSF) of protein residues; (d) distance between ligand and binding site center; (e) buried solvent-accessible surface area (SASA) between ligand and protein; (f) superposition of MD trajectories; (g) van der Waals (VDW) and electrostatic (ELE) energy components of binding; (h) energy contribution of key amino acid residues; (i) number of hydrogen bonds formed during simulation; (j) schematic of protein-ligand interaction mode. All docking scores <–5.0 kcal·mol^{-1}, indicating stable binding affinity.

2.576 in MKN-45 cells (Fig. 3E,F). Kaempferol combined with erlotinib or apatinib has a greater inhibitory effect on cell growth than either drug alone does, demonstrating a synergistic effect. The concentrations of kaempferol (5–60 μM), erlotinib (10.625–127.5 μM), and apatinib (4.75–57 μM) were selected on the basis of their IC_{50} values in MKN-45 and HGC-27 cells (Fig. 3A,B). These ranges encompass subinhibitory concentrations (20–50% of the IC_{50}) to ensure measurable combinatorial effects, which is consistent with the ZIP synergy analysis methodology [14]. Although baseline sensitivities differ (e.g., HGC-27 IC_{50}: 22.64–71.40 μM vs. MKN-45: 77.21–134.7 μM), standardized ranges enable direct comparisons of synergy scores across cell lines.

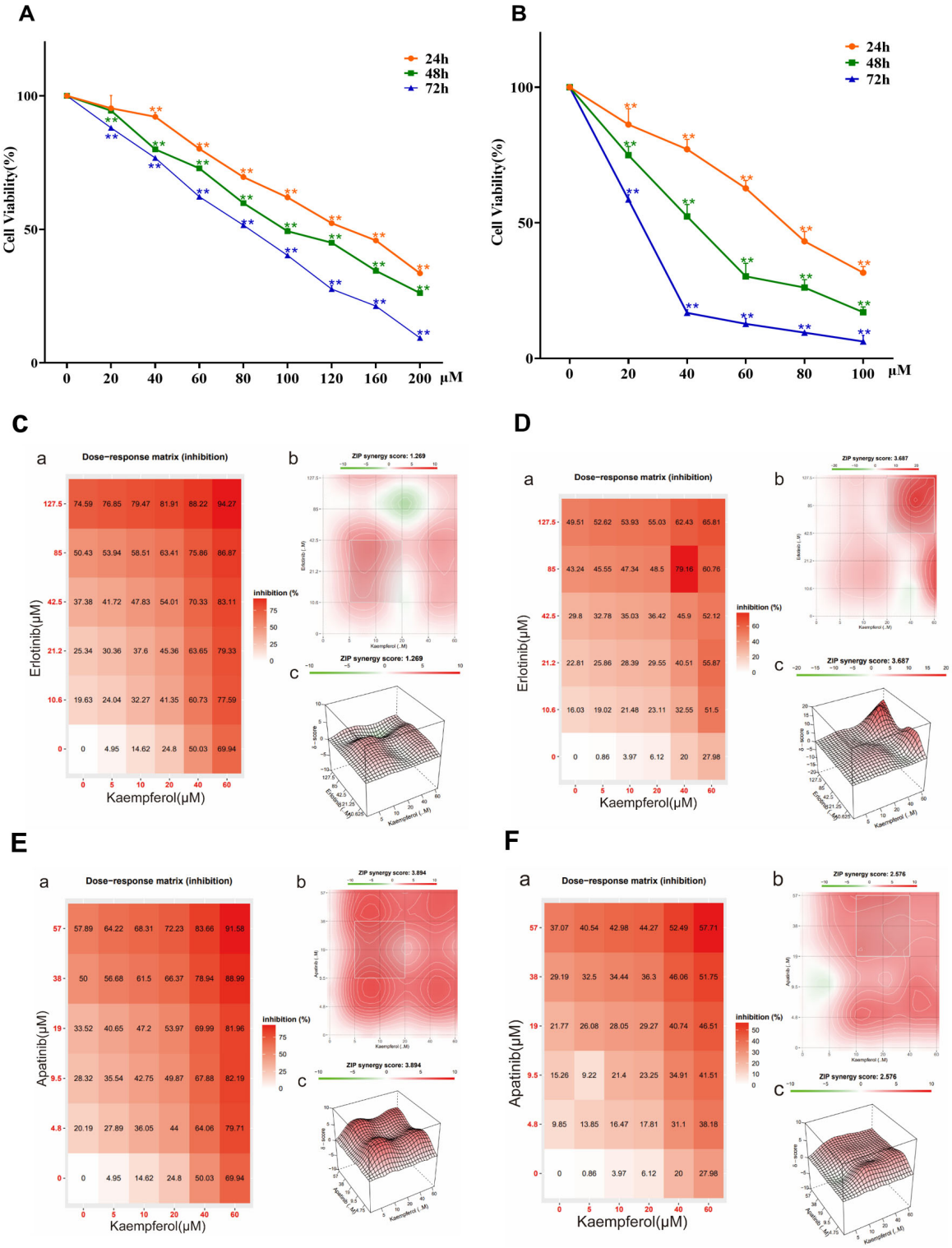


Fig. 3. Synergistic effects of kaempferol combined with apatinib and erlotinib on GC cell viability. (A) Dose- and time-dependent inhibitory effect of kaempferol on MKN-45 cell viability (**$p < 0.01$ vs control). (B) Dose- and time-dependent inhibitory effect of kaempferol on HGC-27 cell viability (*$p < 0.05$, **$p < 0.01$ vs control). (C,D) Synergistic effect of kaempferol combined with erlotinib: (C) HGC-27 cells (zero-interaction potency (ZIP) synergy score = 1.269) (a–c), (D) MKN-45 cells (ZIP synergy score = 3.687) (a–c). (E,F) Synergistic effect of kaempferol combined with apatinib: (E) HGC-27 cells (ZIP synergy score = 3.894) (a–c), (F) MKN-45 cells (ZIP synergy score = 2.576) (a–c). Subpanels (a-c) represent dose-response matrix, 2D synergy heatmap, and 3D synergy landscape, respectively.

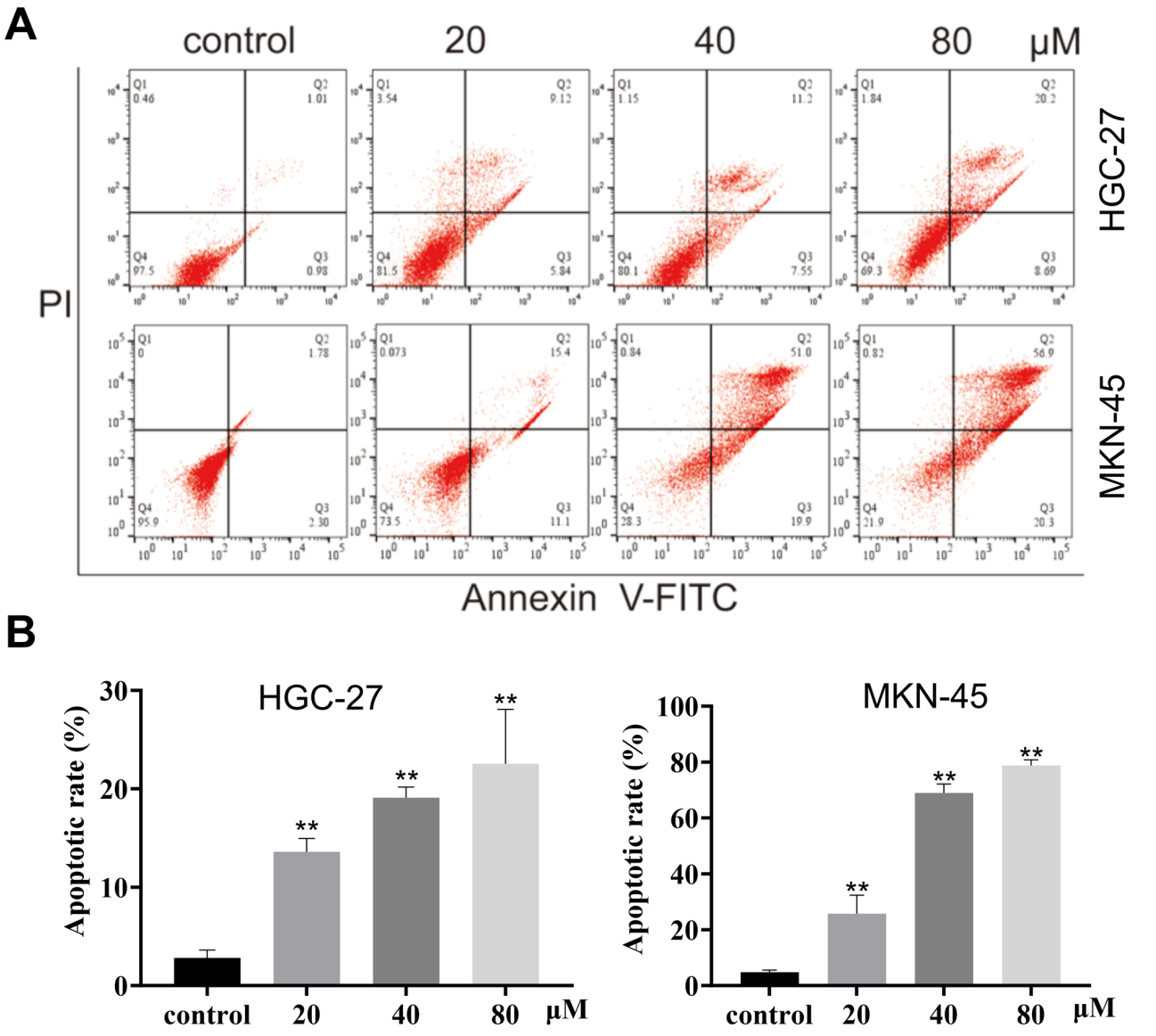


Fig. 4. The influences of kaempferol on apoptosis of GC cells. Flow cytometric analysis of kaempferol-induced apoptosis in GC cells: (A) representative flow cytometry plots for both cell lines (HGC-27 in the top row and MKN-45 in the bottom row), (B) corresponding apoptosis quantification for both cell lines (HGC-27 on the left and MKN-45 on the right). Cells were treated with 20, 40, 80 μM kaempferol for 48 h; the right lower quadrant represents early apoptotic cells, and the right upper quadrant represents late apoptotic cells (**$p < 0.01$ vs control).

3.7 Kaempferol Induces Apoptosis and Cell Cycle Arrest in GC Cells

Using flow cytometry, the pro-apoptotic effect of kaempferol was assessed. When HGC-27 and MKN-45 cells were treated with kaempferol (20, 40, and 80 μM) for 48 hours, apoptosis was dramatically increased in a dose-dependent manner ($p < 0.05$) (Fig. 4A,B). Simultaneously, cell cycle analysis showed that kaempferol administration significantly arrested both cell lines during the G0/G1 phase, thereby modulating cell cycle progression (Fig. 5A,B).

3.8 Molecular Mechanisms Underlying Kaempferol's Effects on Cell Cycle and Apoptosis

The expression of important regulatory proteins was examined in order to clarify the molecular mechanisms. While the anti-apoptotic protein Bcl-2 was downregulated, kaempferol therapy increased the mRNA and protein levels of the pro-apoptotic component Bax and the tumor suppressor P53. As a result, the Bax/Bcl-2 ratio significantly increased, which encouraged apoptosis mediated by the mitochondrial route. Concurrently, kaempferol induced G0/G1 phase cell cycle arrest by upregulating P21 and downregulating CDK4 and CDK6, as shown in Fig. 6A–C.

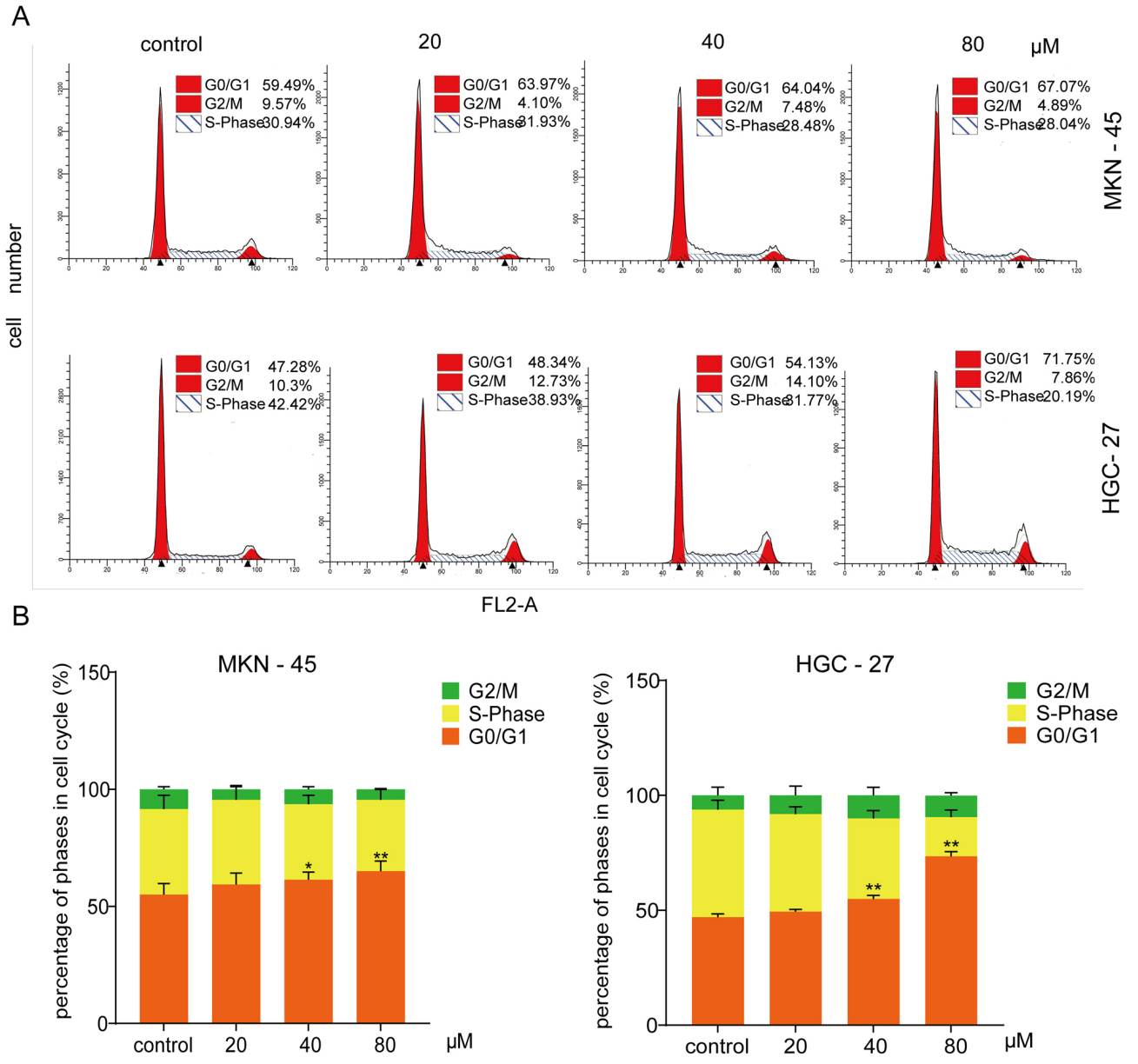


Fig. 5. The influences of kaempferol on cell cycle of GC cells. Flow cytometric analysis of kaempferol-induced G0/G1 phase cell cycle arrest in GC cells: (A) Representative flow cytometric plots for both HGC-27 and MKN-45 cells, (B) Quantification of the G0/G1-phase cell population for both HGC-27 and MKN-45 cells. Cells were treated with 20, 40, 80 μM kaempferol for 48 h; the proportion of G0/G1 phase cells increased significantly in a dose-dependent manner (*$p < 0.05$, **$p < 0.01$ vs control).

3.9 Effects of Kaempferol on the EGFR/PI3K/AKT/mTOR Signaling Pathway

The EGFR/PI3K/AKT/mTOR signaling pathway in GC cells is inhibited by kaempferol, as demonstrated by Western blot analysis, which showed that treatment at 20, 40, and 80 μM for 48 hours significantly lowered the p-PI3K/PI3K, p-AKT/AKT, and p-mTOR/mTOR protein ratios ($p < 0.05$ or 0.01) (Fig. 7A,B).

3.10 Synergistic Effects of Kaempferol, Apatinib, and Erlotinib on the PI3K/AKT/mTOR Signaling Pathway

The effects of the combination of kaempferol (20 μM) and apatinib (19 μM) on the expression of VEGFR2, VEGFA, p-PI3K, and p-AKT in GC cells MKN-45 (a) and HGC-27 (b) were detected for 48 hours.

Kaempferol (20 μM) and apatinib (19 μM) were administered either separately or in combination to GC cells based on the predefined IC_{50} values to achieve sub-inhibitory concentrations (approximately 15–35% inhibition for apatinib and ~50% inhibition for kaempferol at 48 h as single agents). These therapies dramatically de-

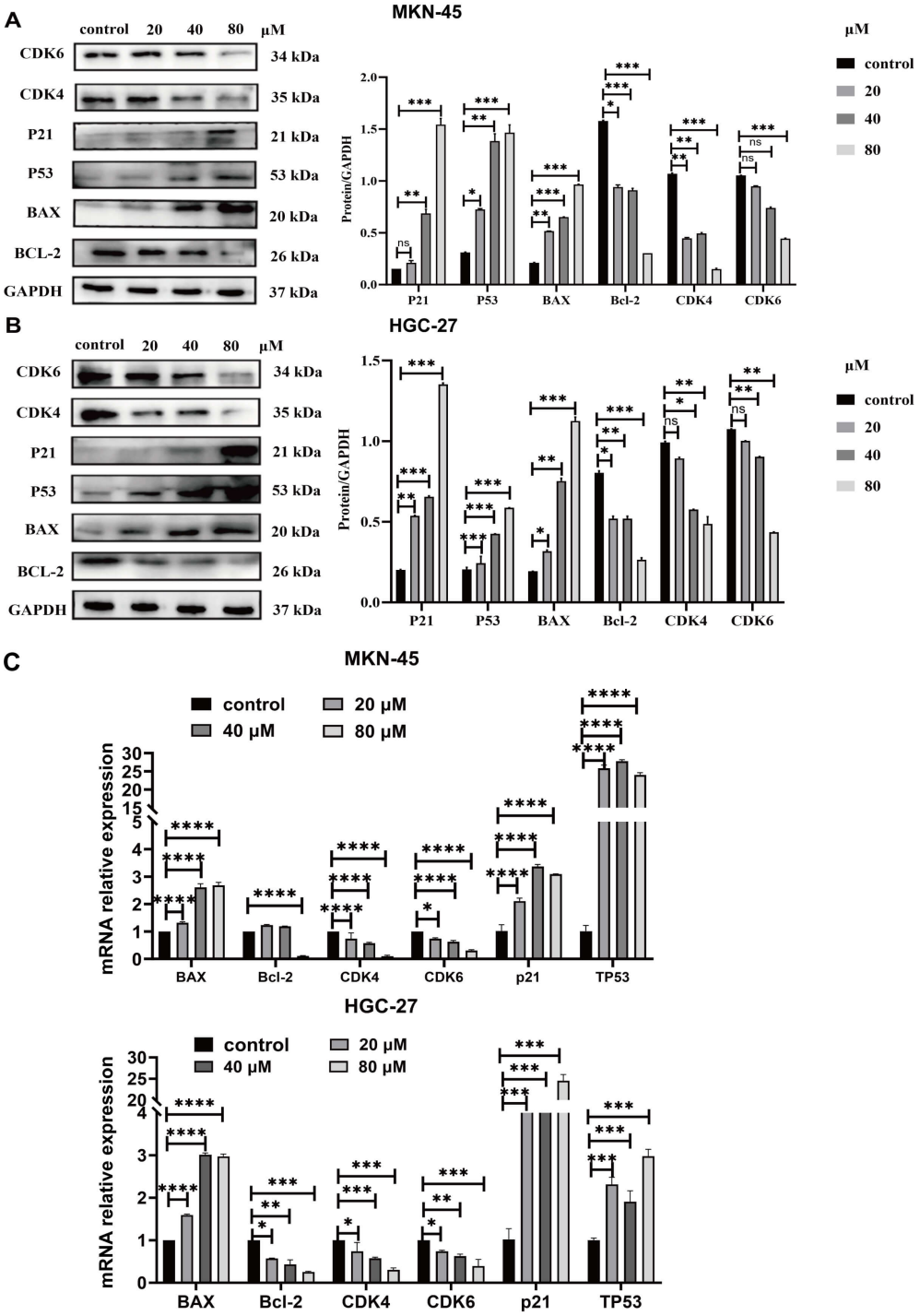


Fig. 6. Effects of kaempferol on apoptosis- and cell cycle-related protein and mRNA expression in gastric cancer cells. (A) Western blot analysis and protein quantification of apoptosis- and cell cycle-related proteins in kaempferol-treated MKN-45 cells. (B) Western blot analysis and protein quantification of apoptosis- and cell cycle-related proteins in kaempferol-treated HGC-27 cells. (C) RT-qPCR validation of mRNA expression of pro-apoptotic genes (*Bax*, *p53*, *p21*) and anti-apoptotic/cycle-promoting genes (*Bcl-2*, *CDK4*, *CDK6*) in both MKN-45 and HGC-27 cells. Kaempferol upregulated pro-apoptotic mRNAs and downregulated anti-apoptotic mRNAs (*$p < 0.05$, **$p < 0.01$, ***$p < 0.001$, ****$p < 0.0001$ vs control).

creased VEGFR2 and VEGFA protein levels and decreased the phosphorylation of PI3K and AKT (p-PI3K, p-AKT) ($p < 0.05$), according to Western blot examination. This suggests that the PI3K/AKT signaling pathway is being suppressed. All of these results point to the regulation of the VEGF/PI3K/AKT signaling pathway as the mechanism by

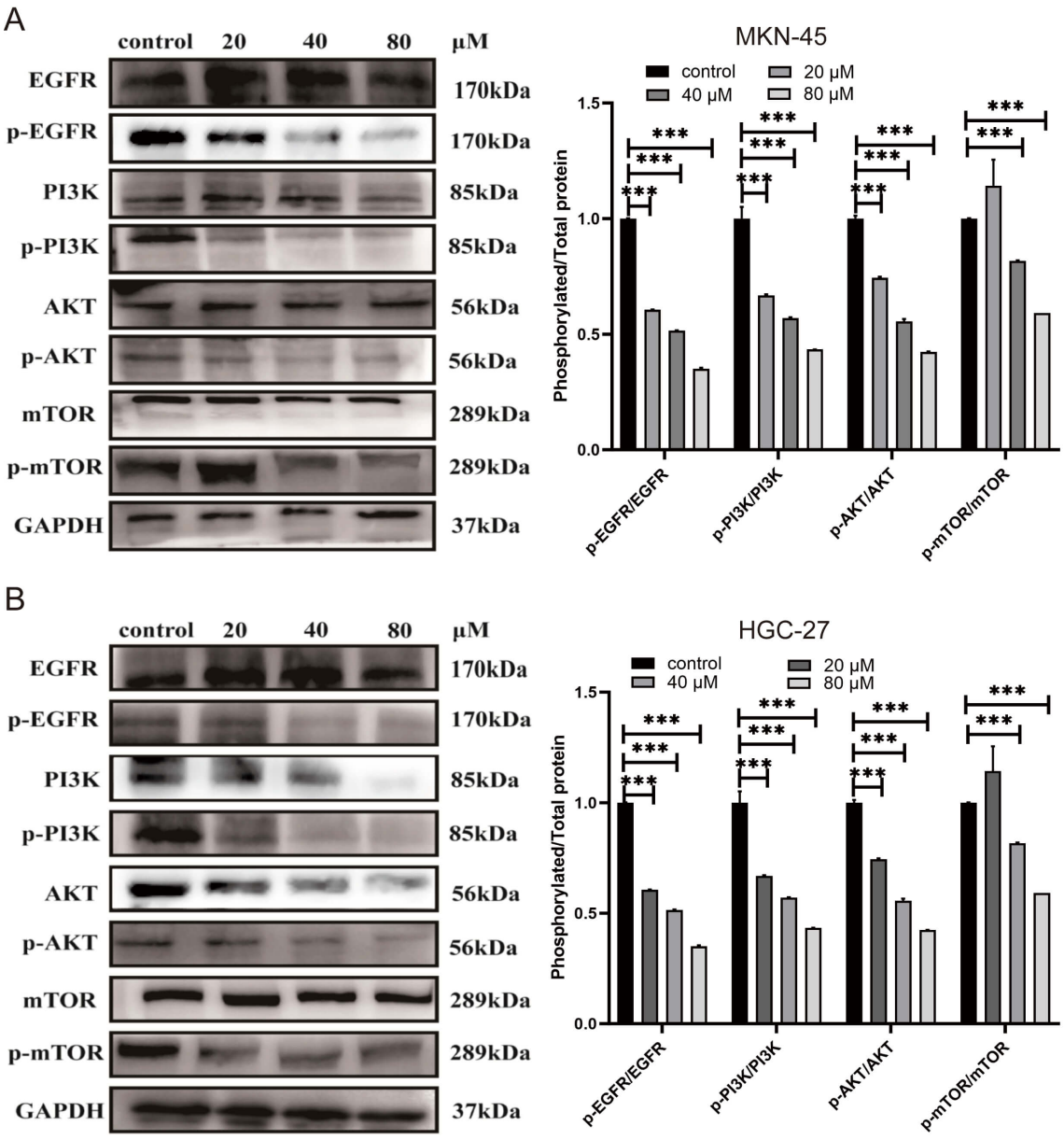


Fig. 7. The effects of kaempferol on EGFR/PI3K/AKT/mTOR signaling pathway. Effect of kaempferol on EGFR/PI3K/AKT/mTOR pathway activation in GC cells: (A) MKN-45 cells, (B) HGC-27 cells. Cells were treated with 20–80 μM kaempferol for 48 h; kaempferol significantly reduced phosphorylation ratios of EGFR, PI3K, AKT, and mTOR (***$p < 0.001$ vs control).

which kaempferol and apatinib limit the development of GC cells. The effects of the combination of kaempferol (20 μM) and erlotinib (42.5 μM) were detected for 48 hours. To activate the PI3K/AKT/mTOR signaling pathway, epidermal growth factor (EGF) at a concentration of 20 ng/mL was applied to GC cells for 30 minutes to induce EGFR activation prior to sample collection. Kaempferol decreased protein levels of p-EGFR and p-AKT ($p < 0.05$). These results suggest decreased phosphorylation of EGFR and AKT proteins in cancer cells. The phosphorylation of the EGFR and AKT proteins was decreased by kaempferol and erlotinib alone or in combination ($p < 0.05$ or 0.01). Kaempferol and apatinib (Fig. 8A) or erlotinib (Fig. 8B) stop the growth of GC cells by controlling downstream signaling pathways and inhibiting EGFR phosphorylation (Fig. 8A,B).

4. Discussion

GC continues to be a serious public health concern, ranking as the second most frequent cancer in men and fifth in women in terms of incidence and mortality. *Helicobacter pylori* (*Hp*) infection represents a key risk factor for GC development in high-risk populations [16,17]. Traditional Chinese medicine (TCM) has shown therapeutic potential in managing *H. pylori*-associated chronic atrophic gastritis, a precancerous lesion associated with gastric cancer [18]. Additionally, extracts of *Marsdenia tenacissima* have been

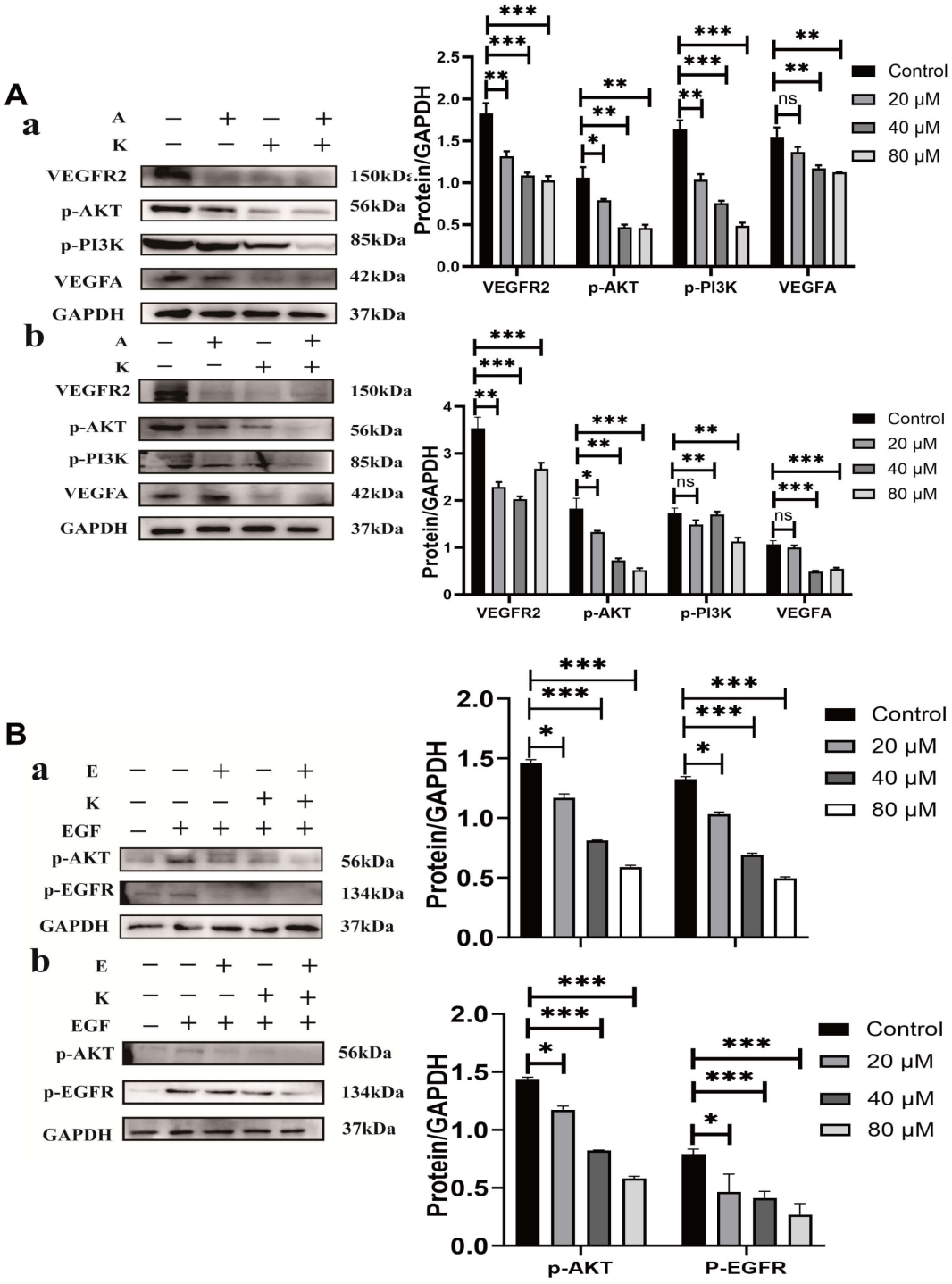


Fig. 8. Kaempferol inhibits epidermal growth factor (EGF)-induced phosphorylation of EGFR and AKT in MKN-45 and HGC-27 GC cells. Synergistic inhibitory effect of kaempferol combined with targeted agents on downstream signaling: (A) Kaempferol (20 μM) + apatinib (19 μM) reduced VEGFR2, VEGFA, p-PI3K, and p-AKT expression in (a) MKN-45 and (b) HGC-27 cells. (B) Kaempferol (20 μM) + erlotinib (42.5 μM) reduced p-EGFR and p-AKT expression in (a) MKN-45 and (b) HGC-27 cells. EGF (20 ng/mL) was used to pre-activate the pathway prior to treatment (*$p < 0.05$, **$p < 0.01$, ***$p < 0.001$ vs control).

reported to reverse resistance to erlotinib and gefitinib, both *in vitro* and *in vivo*, through modulation of Axl and c-Met signaling pathways [19].

KEGG enrichment study suggested that kaempferol may influence the onset and progression of GC by targeting the EGFR receptor resistance signaling pathway, which controls various cellular physiological processes, includ-

ing induction of autophagy, reduction in oxidative stress, and resistance to lipid peroxidation [20,21]. The network pharmacology results of this investigation revealed that the EGFR/PI3K/AKT/mTOR signaling pathway is abundant in the key proteins EGFR and AKT1, with EGFR being intimately associated with the onset and progression of GC. Our experiments confirmed that kaempferol could suppress proliferation, promote apoptosis, and halt the cell cycle at the G0/G1 stage with a concentration-dependent effect via the EGFR/PI3K/AKT/mTOR pathway. Furthermore, the combination of kaempferol with apatinib exhibited synergistic effects against GC cells. These results demonstrate that targeting the EGFR/PI3K/AKT/mTOR signaling pathway may increase the susceptibility of GC cells to small-molecule targeted medicines. Beyond EGFR, other receptor tyrosine kinases also represent therapeutic targets in GC. HER2 status is inversely correlated with tumor invasion depth, suggesting its potential as an early molecular marker in gastric carcinogenesis [22]. The success of HER2-targeted therapy (e.g., trastuzumab) in HER2-amplified/overexpressing GC has highlighted the value of such therapeutic strategies [23]. However, resistance to targeted therapies remains a challenge due to a lack of effective alternative agents [24]. Nevertheless, an initial analysis of 363 screened patients revealed EGFR amplification in 19 (5%) patients with GC; the addition of cetuximab to their chemotherapy significantly increased the tumor response rate [25]. These findings suggest that individuals with GC who have EGFR gene amplification but not EGFR gene mutation might benefit from anti-EGFR therapy [26]. In GC therapy, the VEGF/VEGFR pathway serves as a key angiogenic driver, making it a primary target. A Phase III trial demonstrated that apatinib monotherapy improves overall survival in heavily pretreated patients [27].

Our study demonstrated that kaempferol synergizes with erlotinib and apatinib to inhibit GC cell proliferation, likely through dual suppression of the EGFR and VEGF signaling pathways. This finding aligns with the report that kaempferol sensitizes pancreatic cancer cells to erlotinib via EGFR/PI3K/AKT allosteric modulation [9]. Importantly, we propose a novel strategy whereby concurrent suppression of both axes may disrupt the compensatory signaling that drives resistance to single-agent therapy. Contemporary pharmacological research has demonstrated that kaempferol can decrease cell growth [8,28]. In certain malignancies, it inhibits cell invasion and migration [29,30] and induces cell death [31]. The serine/threonine kinase AKT1 regulates critical processes, including cell growth, angiogenesis, metabolism, and survival [32]. Tumor vascular bed expansion can be induced by VEGFA, which is produced in tumors by hypoxic tumor cells, endothelial cells, and invading bone marrow cells [33]. The HER family protein EGFR is a crucial cellular process regulator and has significant prognostic value across various solid tumors [34].

Erlotinib, a tyrosine kinase inhibitor targeting EGFR, has limited efficacy due to adverse effects and drug resistance. Consequently, our results suggest that kaempferol combined with erlotinib could suppress the proliferation of GC cells and reduce EGFR/AKT phosphorylation levels. Kaempferol enhances the efficacy of the VEGFR inhibitor apatinib in GC by concurrently targeting complementary pathways. It potentiates apatinib's antiangiogenic effect by suppressing VEGFR2/VEGFA expression.

Mechanistically, EGF stimulation upregulates VEGFA via PI3K/Akt and MAPK/ERK pathways [35], creating a PI3K-dependent positive feedback loop through VEGFR2 that amplifies pro-survival signaling. Kaempferol counteracts this by suppressing Hypoxia-inducible factor 1-alpha (HIF-1α) and Akt to reduce VEGFA transcription, while directly inhibiting VEGFR2 phosphorylation and its downstream cascades [36]. Preclinical evidence indicates that apatinib enhances the antitumor activity of EGFR-TKIs in NSCLC models with EGFR-TKI resistance [37], potentially countering adaptive resistance. Thus, the kaempferol-apatinib combination synergistically inhibits the VEGFR2/PI3K/Akt/mTOR axis through complementary upstream (kaempferol: VEGFA biosynthesis, Akt) and downstream (apatinib: receptor blockade) mechanisms, thereby disrupting the EGFR-VEGFR2 crosstalk. This rationale is supported by clinical evidence showing combined EGFR/VEGF inhibition improves outcomes in Non-Small Cell Lung Cancer (NSCLC) [38,39]. Furthermore, kaempferol independently inhibits the EGFR/PI3K/AKT/mTOR cascade, synergizes with both erlotinib and apatinib, and promotes apoptosis and G0/G1 arrest, collectively suppressing GC cell growth.

5. Conclusion

In summary, our results establish kaempferol as a dual-pathway modulator that synergizes with erlotinib (ZIP scores: 1.269–3.687) and apatinib (ZIP scores: 2.576–3.894) to overcome therapeutic resistance in GC. Molecular dynamics simulations (MM-PBSA) indicate that van der Waals interactions dominate its binding to targets such as PI3K (ΔE_{vdw} = –159.842 ± 2.733 kcal·mol^{-1}; Table 2), suggesting stable hydrophobic packing. Functionally, kaempferol concurrently inhibits the EGFR and VEGFR2 signaling axes, blocks the PI3K/AKT/mTOR pathway, induces G0/G1 cell cycle arrest, and promotes apoptosis via modulation of Bcl-2/Bax, P53, and CDK4/6. This study provides the first evidence for kaempferol's chemosensitizing effect through dual-pathway suppression, offering a theoretical basis for developing natural adjuvant therapies for GC. Future studies in relevant genetically engineered models are warranted to validate these findings *in vivo* and further elucidate the precise causal mechanisms underlying the observed synergistic effects.

6. Limitations

Several limitations should be acknowledged. First, all validations were confined to two GC cell lines (HGC-27, MKN-45) *in vitro*; the absence of *in vivo* xenografts and clinical samples limits translational inference and leaves kaempferol's pharmacokinetics and tolerability unexamined. Second, EGFR/VEGFR2 targeting was identified via network pharmacology, molecular docking, and MD simulations—predictive by nature—without direct binding confirmation (e.g., SPR, ITC, or site-directed mutagenesis). Third, conclusions derive from only two cell lines, limiting generalizability across GC molecular subtypes (EBV-positive, MSI, genomically stable, chromosomal instability), and kaempferol's selectivity toward tumor versus normal gastric epithelium was not assessed. Fourth, some apatinib and erlotinib IC50 values exceeded the highest tested concentration (100 μM) and were extrapolated, reducing precision. Finally, synergy was inferred from pathway modulation rather than formal combination-index (Chou–Talalay) or rescue analyses establishing causal directionality of the EGFR/VEGFR2 crosstalk. Future *in vivo* and mechanistic studies are needed before clinical translation.

Availability of Data and Materials

The data that support the findings of this study are available from the corresponding author upon reasonable request.

Author Contributions

(I) Conception and design: HL; (II) Administrative support: HW, YH; (III) Provision of study materials or patients: HL and YH, MW and RS; (IV) Collection and assembly of data: MW, RS and LS; (V) Data analysis and interpretation: HL YH and HW; (VI) Manuscript writing: MW wrote the first draft of the manuscript, which was revised by HL. All authors contributed to editorial changes in the manuscript. All authors read and approved the final manuscript. All authors have participated sufficiently in the work and agreed to be accountable for all aspects of the work.

Ethics Approval and Consent to Participate

Not applicable.

Acknowledgment

Not applicable.

Funding

This work was supported by the following grant numbers: Gansu Province Traditional Chinese Medicine Research Project (GZKG-2022-53), Innovation Fund Project of Affiliated Hospital of Gansu University of Chinese Medicine (gzfy-2021-01), and General program of Shenzhen Natural Science Foundation (JCYJ20250604190013017).

Conflicts of Interest

The authors declare no conflicts of interest.

References

[1] Arnold M, Abnet CC, Neale RE, Vignat J, Giovannucci EL, McGlynn KA, et al. Global Burden of 5 Major Types of Gastrointestinal Cancer. Gastroenterology. 2020; 159: 335–349.e15. https://doi.org/10.1053/j.gastro.2020.02.068

[2] Sung H, Ferlay J, Siegel RL, Laversanne M, Soerjomataram I, Jemal A, et al. Global Cancer Statistics 2020: GLOBOCAN Estimates of Incidence and Mortality Worldwide for 36 Cancers in 185 Countries. CA: a Cancer Journal for Clinicians. 2021; 71: 209–249. https://doi.org/10.3322/caac.21660

[3] Wang Y, Zhang Q, Chen Y, Liang CL, Liu H, Qiu F, et al. Antitumor effects of immunity-enhancing traditional Chinese medicine. Biomedicine & Pharmacotherapy = Biomedecine & Pharmacotherapie. 2020; 121: 109570. https://doi.org/10.1016/j.biopha.2019.109570

[4] Cui D, Zhang C, Zhang L, Zheng J, Wang J, He L, et al. Natural anti-cancer products: insights from herbal medicine. Chinese Medicine. 2025; 20: 82. https://doi.org/10.1186/s13020-025-01124-y

[5] Park J, Lee GE, An HJ, Lee CJ, Cho ES, Kang HC, et al. Kaempferol sensitizes cell proliferation inhibition in oxaliplatin-resistant colon cancer cells. Archives of Pharmacal Research. 2021; 44: 1091–1108. https://doi.org/10.1007/s12272-021-01358-y

[6] Li Q, Wei L, Lin S, Chen Y, Lin J, Peng J. Synergistic effect of kaempferol and 5-fluorouracil on the growth of colorectal cancer cells by regulating the PI3K/Akt signaling pathway. Molecular Medicine Reports. 2019; 20: 728–734. https://doi.org/10.3892/mmr.2019.10296

[7] Chen J, Zhang X, Xiao X, Ding Y, Zhang W, Shi M, et al. Xiao-Ai-Ping Injection Enhances Effect of Paclitaxel to Suppress Breast Cancer Proliferation and Metastasis via Activating Transcription Factor 3. Integrative Cancer Therapies. 2020; 19: 1534735420906463. https://doi.org/10.1177/1534735420906463

[8] Amjad E, Sokouti B, Asnaashari S. A systematic review of anticancer roles and mechanisms of kaempferol as a natural compound. Cancer Cell International. 2022; 22: 260. https://doi.org/10.1186/s12935-022-02673-0

[9] Zhang Z, Guo Y, Chen M, Chen F, Liu B, Shen C. Kaempferol potentiates the sensitivity of pancreatic cancer cells to erlotinib via inhibition of the PI3K/AKT signaling pathway and epidermal growth factor receptor. Inflammopharmacology. 2021; 29: 1587–1601. https://doi.org/10.1007/s10787-021-00848-1

[10] Daina A, Michielin O, Zoete V. SwissTargetPrediction: updated data and new features for efficient prediction of protein targets of small molecules. Nucleic Acids Research. 2019; 47: W357–W364. https://doi.org/10.1093/nar/gkz382

[11] Wang Y, Wang Q, Huang H, Huang W, Chen Y, McGarvey PB, et al. A crowdsourcing open platform for literature curation in UniProt. PLoS Biology. 2021; 19: e3001464. https://doi.org/10.1371/journal.pbio.3001464

[12] Otasek D, Morris JH, Bouças J, Pico AR, Demchak B. Cytoscape Automation: empowering workflow-based network analysis. Genome Biology. 2019; 20: 185. https://doi.org/10.1186/s13059-019-1758-4

[13] Zhou Y, Zhou B, Pache L, Chang M, Khodabakhshi AH, Tanaseichuk O, et al. Metascape provides a biologist-oriented resource for the analysis of systems-level datasets. Nature Communications. 2019; 10: 1523. https://doi.org/10.1038/s41467-019-09234-6

[14] Zhang Q, Zhou Y, Feng X, Gao Y, Huang C, Yao X. Low-dose

orlistat promotes the therapeutic effect of oxaliplatin in colorectal cancer. Biomedicine & Pharmacotherapy = Biomedecine & Pharmacotherapie. 2022; 153: 113426. https://doi.org/10.1016/j.biopha.2022.113426

[15] Wang M, Li HL, Ning Y, Shao LH, Gao XQ, Yang CT, et al. The Inhibitory Action and Mechanisms of Marsdenia Tenacissima Oral Liquid on the Proliferation of Gastric Cancer Cells Based on Network Pharmacology and in vitro Experiments and the Sensitization Effect of Combining Erlotinib and Apatinib. Journal of Basic Chinese Medicine. 2024; 30: 1178–1190. (In Chinese)

[16] Burz C, Pop V, Silaghi C, Lupan I, Samasca G. *Helicobacter pylori* Infection in Patients with Gastric Cancer: A 2024 Update. Cancers. 2024; 16: 1958. https://doi.org/10.3390/cancers16111958

[17] Andreev DN, Khurmatullina AR, Maev IV, Bordin DS, Abdulkhakov SR, Kucheryavyy YA, et al. The Prevalence of *Helicobacter pylori* Infection in the Adult Population of Russia: A Systematic Review and Meta-Analysis. Epidemiologia (Basel, Switzerland). 2025; 6: 47. https://doi.org/10.3390/epidemiologia6030047

[18] Wen J, Wu S, Ma X, Zhao Y. Zuojin Pill attenuates Helicobacter pylori-induced chronic atrophic gastritis in rats and improves gastric epithelial cells function in GES-1 cells. Journal of Ethnopharmacology. 2022; 285: 114855. https://doi.org/10.1016/j.jep.2021.114855

[19] Han SY, Zhao W, Han HB, Sun H, Xue D, Jiao YN, et al. *Marsdenia tenacissima* extract overcomes Axl- and Met-mediated erlotinib and gefitinib cross-resistance in non-small cell lung cancer cells. Oncotarget. 2017; 8: 56893–56905. https://doi.org/10.18632/oncotarget.18137

[20] Alrumaihi F, Almatroodi SA, Alharbi HOA, Alwanian WM, Alharbi FA, Almatroudi A, et al. Pharmacological Potential of Kaempferol, a Flavonoid in the Management of Pathogenesis via Modulation of Inflammation and Other Biological Activities. Molecules (Basel, Switzerland). 2024; 29: 2007. https://doi.org/10.3390/molecules29092007

[21] Levantini E, Maroni G, Del Re M, Tenen DG. EGFR signaling pathway as therapeutic target in human cancers. Seminars in Cancer Biology. 2022; 85: 253–275. https://doi.org/10.1016/j.semcancer.2022.04.002

[22] Senel F. Clinicopathologic significance of human epidermal growth factor receptor 2 expression and gene amplification in gastric carcinoma. Journal of Cancer Research and Therapeutics. 2022; 18: S299–S304. https://doi.org/10.4103/jcrt.JCRT_1810_20

[23] Kawakami T, Yamazaki K. Recent Progress in Treatment for HER2-Positive Advanced Gastric Cancer. Cancers. 2024; 16: 1747. https://doi.org/10.3390/cancers16091747

[24] Mo C, Sterpi M, Jeon H, Bteich F. Resistance to Anti-HER2 Therapies in Gastrointestinal Malignancies. Cancers. 2024; 16: 2854. https://doi.org/10.3390/cancers16162854

[25] Maron SB, Alpert L, Kwak HA, Lomnicki S, Chase L, Xu D, et al. Targeted Therapies for Targeted Populations: Anti-EGFR Treatment for *EGFR*-Amplified Gastroesophageal Adenocarcinoma. Cancer Discovery. 2018; 8: 696–713. https://doi.org/10.1158/2159-8290.CD-17-1260

[26] Lei ZN, Teng QX, Tian Q, Chen W, Xie Y, Wu K, et al. Signaling pathways and therapeutic interventions in gastric cancer. Signal Transduction and Targeted Therapy. 2022; 7: 358. https://doi.org/10.1038/s41392-022-01190-w

[27] Li J, Qin S, Xu J, Xiong J, Wu C, Bai Y, et al. Randomized, double-blind, placebo-controlled phase III trial of apatinib in patients with chemotherapy-refractory advanced or metastatic adenocarcinoma of the stomach or gastroesophageal junction. Journal of Clinical Oncology. 2016; 34: 1448–1454. https://doi.org/10.1200/JCO.2015.63.5995

[28] Wang F, Wang L, Qu C, Chen L, Geng Y, Cheng C, et al. Kaempferol induces ROS-dependent apoptosis in pancreatic cancer cells via TGM2-mediated Akt/mTOR signaling. BMC Cancer. 2021; 21: 396. https://doi.org/10.1186/s12885-021-08158-z

[29] Sugita S, Matsuo Y, Ishida M, Uehara Y, Eguchi Y, Denda Y, et al. Kaempferol Inhibits MMP-1-Mediated Migration and Invasion in Gemcitabine-Resistant Pancreatic Cancer Cells. Nutrients. 2026; 18: 380. https://doi.org/10.3390/nu18030380

[30] Gao XQ, Li HL, Wang M, Yang CT, Su R, Shao LH. Kaempferol inhibited invasion and metastasis of gastric cancer cells by targeting AKT/GSK3β pathway based on network pharmacology and molecular docking. Journal of Asian Natural Products Research. 2025; 27: 421–441. https://doi.org/10.1080/10286020.2024.2387756

[31] Gao X, Liang Q, Su R, Qiu S, Jing Z, Chen F, et al. Kaempferol Triggers Ferroptosis of Gastric Cancer Cells by the P53/SLC7A11/GPX4 Pathway Based on PCR Array and In Vitro Experiments. Journal of Pioneering Medical Sciences. 2025; 14: 55–66. https://doi.org/10.47310/jpms2025141209

[32] Leiphrakpam PD, Batra R, Tenner L, Are C. Targeting Akt Signaling Pathway in Cancer: Molecular Mechanisms and Advances in Therapeutic Interventions. Frontiers in Bioscience (Landmark Edition). 2025; 30: 39100. https://doi.org/10.31083/FBL39100

[33] Shi Z, Kuai M, Li B, Akowuah CF, Wang Z, Pan Y, et al. The role of VEGF in Cancer angiogenesis and tumorigenesis: Insights for anti-VEGF therapy. Cytokine. 2025; 189: 156908. https://doi.org/10.1016/j.cyto.2025.156908

[34] Lu X, Li Y, Li Y, Zhang X, Shi J, Feng H, et al. Prognostic and predictive biomarkers for anti-EGFR monoclonal antibody therapy in RAS wild-type metastatic colorectal cancer: a systematic review and meta-analysis. BMC Cancer. 2023; 23: 1117. https://doi.org/10.1186/s12885-023-11600-z

[35] Hung MS, Chen IC, Lin PY, Lung JH, Li YC, Lin YC, et al. Epidermal growth factor receptor mutation enhances expression of vascular endothelial growth factor in lung cancer. Oncology Letters. 2016; 12: 4598–4604. https://doi.org/10.3892/ol.2016.5287

[36] Kim GD. Kaempferol inhibits angiogenesis by suppressing HIF-1α and VEGFR2 activation via ERK/p38 MAPK and PI3K/Akt/mTOR signaling pathways in endothelial cells. Preventive Nutrition and Food Science. 2017; 22: 320–326. https://doi.org/10.3746/pnf.2017.22.4.320

[37] Li F, Zhu T, Cao B, Wang J, Liang L. Apatinib enhances antitumour activity of EGFR-TKIs in non-small cell lung cancer with EGFR-TKI resistance. European Journal of Cancer. 2017; 84: 184–192. https://doi.org/10.1016/j.ejca.2017.07.037

[38] Nakagawa K, Garon EB, Seto T, Nishio M, Ponce Aix S, Paz-Ares L, et al. Ramucirumab plus erlotinib in patients with untreated, EGFR-mutated, advanced non-small-cell lung cancer (RELAY): a randomised, double-blind, placebo-controlled, phase 3 trial. The Lancet Oncology. 2019; 20: 1655–1669. https://doi.org/10.1016/S1470-2045(19)30634-5

[39] Wang Q, Zeng A, Zhu M, Song L. Dual inhibition of EGFR-VEGF: An effective approach to the treatment of advanced non-small cell lung cancer with EGFR mutation (Review). International Journal of Oncology. 2023; 62: 26. https://doi.org/10.3892/ijo.2023.5474